

Article

The Suitability of UAS for Mass Movement Monitoring Caused by Torrential Rainfall—A Study on the Talus Cones in the Alpine Terrain in High Tatras, Slovakia

Rudolf Urban ^{1,*}, Martin Štroner ¹, Peter Blistan ² , Ľudovít Kovanič ² , Matej Patera ², Stanislav Jacko ³, Igor Ďuriška ³, Miroslav Kelemen ⁴  and Stanislav Szabo ⁴

¹ Department of Special Geodesy, Faculty of Civil Engineering, Czech Technical University in Prague, Thákurova 7, 166 29 Prague, Czech Republic

² Institute of Geodesy, Cartography and Geographical Information Systems, Faculty of Mining, Ecology, Process Control and Geotechnology, Technical University Kosice, Park Komenského 19, 04001 Košice, Slovakia

³ Institute of Geosciences, Faculty of Mining, Ecology, Process Control and Geotechnology, Technical University Kosice, Park Komenského 15, 04001 Košice, Slovakia

⁴ Department of Flight Training, Faculty of Aeronautics, Technical University of Kosice, Ramp 7, Kosice 04121, Slovakia

* Correspondence: rudolf.urban@fsv.cvut.cz

Received: 8 May 2019; Accepted: 20 July 2019; Published: 24 July 2019



Abstract: The prediction of landslides and other events associated with slope movement is a very serious issue in many national parks around the world. This article deals with the territory of the Malá Studená Dolina (Little Cold Valley, High Tatras National Park—Slovakia), where there are extensive talus cones, through which seasonally heavy hiking trails lead. In the last few years particularly, there have been frequent falls and landslides in the mountainous environment, which also caused several fatal injuries in 2018. For the above reasons, efforts are being made to develop a methodology for monitoring the changes of the talus cones in this specific alpine area, to determine the size, speed, and character of the morphological changes of the soil. Non-contact methods of mass data collection (laser scanning with Leica P40 and aerial photogrammetry with unmanned aerial system (UAS) DJI Phantom 4 Pro) have been used. The results of these measurements were compared and the overall suitability of both methods for measurement in such terrain evaluated. The standard deviation of the difference of surface determination (represented by the point cloud) is about 0.03 m. As such accuracy is sufficient for the purpose of monitoring talus cones and the use of UAS is easier and associated with lower risk of damage of expensive equipment, we conclude that this method is more suitable for mapping and for repeated monitoring of such terrain. The properties of the outputs of the individual measurement methods, the degree of measurement difficulty and specific measurement conditions in the mountainous terrain, as well as the economy of the individual methods, are discussed in detail.

Keywords: monitoring; georelief; geohazards; talus cones; UAS; TLS; SfM; torrential rainfall

1. Introduction

The alpine terrain with its exposed georelief and climatic conditions supports a wide range of natural processes with various morphodynamic phenomena. Various influences, including water, sunshine, and temperature changes, on the georelief of the high mountains are reflected in the spatial incidence and intensity of morphological processes such as water-, snow-, and frost-induced processes, solifluction, deflation, etc. Many of these processes occur in the highest positions of the ridges and

peaks; others affect the slopes of the valleys and also reach their foot. Nowadays, in view of climate change, monitoring of the dynamics of georelief evolution and its changes is a frequently discussed topic. The choice of an appropriate data collection method from the point of view of the accuracy, technical complexity, cost-efficiency, and overall suitability is of utmost importance. The use of modern methods of non-contact survey, including digital photogrammetry performed by unmanned aerial system (UAS) carriers or terrestrial laser scanning (TLS), appear to bring significant advantages over the traditional methods of geodesy and cartography, such as measurements using total stations [1]. These traditional procedures are not suitable for detailed monitoring of flat or spatially irregular formations as signaling and subsequent measurements of individual points is unjustifiable in terms of time and money (e.g., [2,3]).

Changes in the position of objects, the shape of the terrain, the morphology of landslides or in anything else in the landscape can be determined by the stage method of measurement—i.e., by taking measurements of the area of interest in various time points. Following the baseline measurement, another one is taken either after a pre-set time period or after a significant event (for example, torrential rain) and the differences between both measurements are analyzed.

As photogrammetric methods (or 3D laser scanning) in principle do not directly relate to a global coordinate system (georeferencing), the use of a certain number of ground control points (GCPs) is required by terrestrial geodesy (with georeferencing) or, more often, by GNSS (global navigation satellite systems), with subsequent transformation into terrestrial position and elevation systems.

UASs have been previously used for many applications, including monitoring of changes in the morphology of a volcano [4], landslides [5,6], dam and riverbed erosion [7–9], slow landslides [10], risks associated with surface mining [11], slope stability in the vicinity of railways [12], or speed of glacier movement [13,14].

Commonly achievable accuracy reported in most studies is 5–10 cm. The terrain monitored in those studies is usually smooth, practically free of vegetation or with sparse vegetation only. A less frequently studied problem is the monitoring of areas covered by vegetation, which makes it difficult to determine changes. We rarely read about monitoring changes in terrain morphology and geological phenomena such as rock blocks, glacier moraine, talus cones, and scree cones, located in hard-to-reach but visited mountain areas.

In this paper we present a procedure for documenting and monitoring the talus cone stability, which is a typical geological phenomenon in alpine areas, using the SfM (Structure from Motion) method based on UAS imaging. The National Park of High Tatras is probably the most visited park in Slovakia and the instability of talus cones during times of of torrential rains thus may present a significant danger to the tourists in their vicinity. To be able to monitor the hazards presented by those cones, however, it is necessary to develop inexpensive but effective methods for detailed description of the surface that could be systematically repeated over time. As the use of traditional geodesy methods is unsuitable for this task, the presented paper aims at developing a method for effective and systematic monitoring using UAS. A significant problem of documentation in the alpine environment is posed by the character of the terrain, which is inclined with a slope usually between 20° and 60°, often very rugged, consisting essentially of larger or smaller boulders ranging in sizes from 10 cm to 1 m (often with the occurrence of isolated stone blocks of several meters). For these reasons, more extensive terrain reconnaissance and consistent planning of the flight is necessary so that a continuous surface can be reconstructed from the data. Due to the inclination and ruggedness of the terrain, it is not practically possible to capture the surface by traditional methods of geodesy, which calls for the use of methods of mass data collection. For this reason, terrestrial 3D laser scanning was chosen as the most appropriate comparative method to verify the quality of the digital terrain model obtained from UAS photogrammetry. The goal of the presented research was to analyze and evaluate the overall suitability (accuracy, quality, laboriousness, efficiency, and usability of the tested methodology) of low-cost UAS photogrammetry for the needs of monitoring selected geohazards (such as rock collapses, glacial moraine, stone fields, and talus cones) located in very specific, rugged, and inclined terrains.

The selected area is typical for the medium-high Alpine-type mountains, such as the above-mentioned Alps or Carpathians, on the example of a talus cone located in the Little Cold Valley in High Tatras.

2. Study Area

The area of interest for monitoring changes of georelief by using UAS photogrammetry was a selected area of High Tatras (in the northern part of Slovakia on the border with Poland), namely the part of the Little Cold Valley (Figure 1).

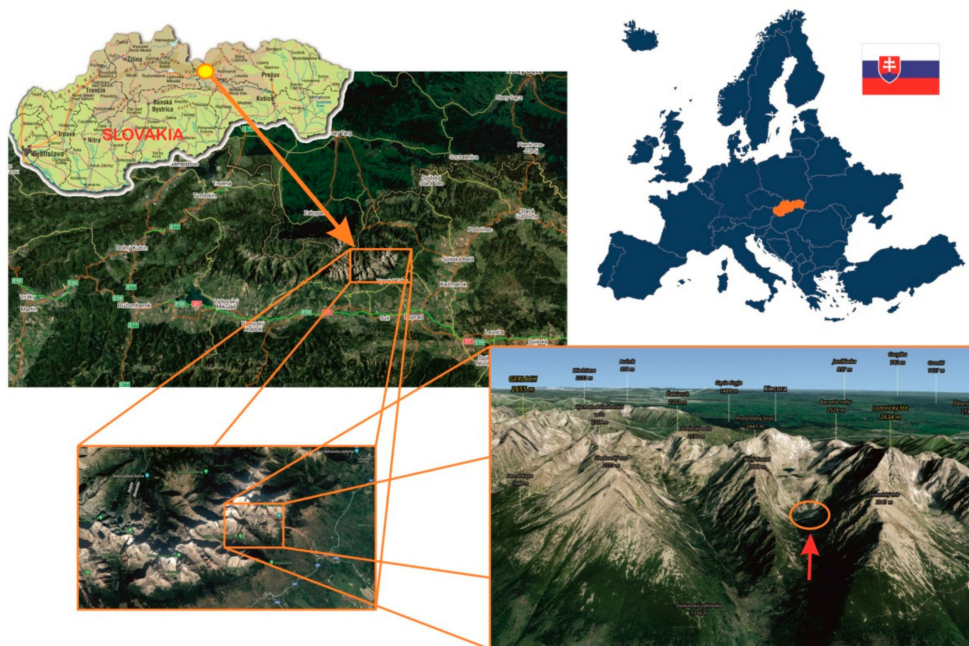


Figure 1. Location—Little Cold Valley in the High Tatras, Slovakia.

The whole territory of the Tatras belongs to the Tatra National Park—TANAP. The area of its own territory is 73,300 ha, and the protection zone is 39,800 ha. TANAP is the highest mountain group in the Carpathian arch. The most valuable part of the area is the 55 km long and 17 km wide geomorphological unit of the Tatras.

The evolution and morphostructural shape of the High Tatras is linked with polyphase tectonic, initialized by Alpine-Carpathian collisional processes that started during the transition from Mesozoic to Cenozoic period and culminated in the Oligocene-Early Miocene by vertical uplift of the mountain range. This robust uplift uncovers Variscan crystalline basement of the Tatric Unit. The younger alpine supra structures such as the Fatric and Hronic Units are conserved only in the marginal parts of the mountains. The Tatric Unit is built by pre-Mesozoic rocks where S-type granodiorites dominate [15,16], respectively medium-grade mica schists. The recent topography of the High Tatras relates to Pleistocene glaciation [17–19] during which 55 glacier systems were created [20] based on the distribution glacial erosional and depositional landforms. The high alpine surface is modified by the processes of weathering, erosion, gravity, and debris flow transport and accumulation [21–25] of granodiorite debris on the sides of the valleys. The debris development is accelerated by the presence of weathering prone mica and an irregular network of faults and joints. The deposits on the talus slopes are positioned on the top of moraine sediments or of floodplain deposits of recent mountain streams that overlap moraine sediments [26] and are built by either proluvial (alluvial), deluvial, or proluvial-deluvial cones. The cones have a typical construction consisting of source, transport, and deposition area. Water transports material in migrating distribution channels, which are often characterized by their "paternoster" structure, where large debris boulders block the channel transport of smaller materials. During massive rainfall events, the strong water inflow causes the boulders to be

released. In the case that accumulation areas of talus slopes are on the floodplain of a recent mountain stream, the deposits are further eroded and carried away from the valley by the stream during the increased water period. The inactive areas of talus slopes are afforested with dwarf mountain pine.

The high alpine surface of the High Tatras is typical for younger morphostructures of the Alpine and Carpathian belt. It is characterized by ragged, steep, high relief valleys filled by regolith. These valleys are developed in glacial or glacial conditions. Recently, several studies have shown that the modern evolution of European high alpine surfaces is closely related to climate change [27–29], especially to temperature anomalies and the increase of intense rainfall events.

The character of the climate is a transitional character between oceanic western European and continental climate, where the cold climatic region of the alpine type prevails. According to the Köppen Climate Classification System, the area belongs to the ET (tundra) climate region [30]. The snow cover stays for 200–250 days a year—in firn areas the whole year. Even in summer, precipitations are often in the form of snow in altitudes above 2000 m. More than 200 days a year, the average daily temperature is below 0 °C.

In the whole area of interest, there are several geomorphological formations of the character of rubble streams, which are increasingly active due to enormous rainfall in the last 10 years. They can potentially be included in geohazards because they are located in the tourist-frequented valleys of the High Tatras (frequented high mountain hiking trails often pass through these places).

The biggest mass movements and talus cones are in Tatras located at the end of trough valleys because these have the highest walls modeled by glaciers. Here, often, talus cones are joined together with alluvial cones to form combined-type alluvial talus cones. The features of such a combined cone are also present in the highest talus cone in the Tatras located at the end of the Kolová Valley under the NE wall of the Kolový Peak. It is 430 m high with water-flooded foot reaching the Kolové tarn (1565 m above sea level). Major talus cones can be also found in [26]:

- The Small Cold Valley, 400 m high;
- Mengusovska Valley below Satan Peak with a height of 400 m;
- East of Vareškove tarn with a height of 330 m.

The author considers enormously high talus cones to be those that exceed 200 m. The same types of talus cones are observable in the Alps, and respectively in all alpine-type mountains.

Mass Movement as a Significant Phenomenon of the Alpine Type Mountains

According to [31], under the term mass movement, we understand the geomorphological process as well as the forms formed under the influence of short-term atmospheric precipitation in the talus material. Precipitation of more than 1 mm·min⁻¹ and yields of 40 mm/day accelerate the movement of debris material on the slopes in the Tatras. While in the Alps mass movements of 400,000–500,000 m³ have been recorded, in the Tatras it is up to 25,000 m³, and in Scotland and Scandinavia only 100–350 m³ [31,32]. Their size is determined by both morphometric and lithological properties. In this case, it is useful to know the debris cover. Statistical measurements show that hourly rainfall intensities of 60–80 mm occur in the Tatras with a probability of 1%—i.e., once every hundred years. However, an intensity of 40 mm·h⁻¹ may occur with a probability of 10%—i.e., once every 10 years. Over the past seven years, the intensity of extreme rainfall has risen compared to the earlier measurements carried out by [33]. As reported by [31], since 1995 in the Tatra Mountains the transition to a more humid climate with the development of fluvial processes is observed, i.e., manifestations of overland flow and concentrated surface runoff in the form of rain rills and washout channels. At present, we observe very active talus cones (seasonal changes are visible by the naked eye) in the area of the Mlynická Valley, Mengusovská Valley, Maple Valley, Great and Little Cold Valley.

Negative manifestations of massive mass movement, such as the destruction of the tourist track located below the face wall of the Lomnický Peak, are well apparent in the Little Cold Valley. The source area starts at an altitude of approximately 2200 m and the width of mass movement was approximately

1250 m in 2014, which is 50 m more than in 2004. Its width in the accumulation zone also increased from the original 5–12 m to 96 m. The same changes in the morphology of mass movement, which is the subject of our research, lie in the close proximity to a previously mentioned mass movement with the source area below Lomnický Peak, documented in the images from 2010 and 2016 (Figure 2). There is also an increase in the length and width of the mass movement over the years.

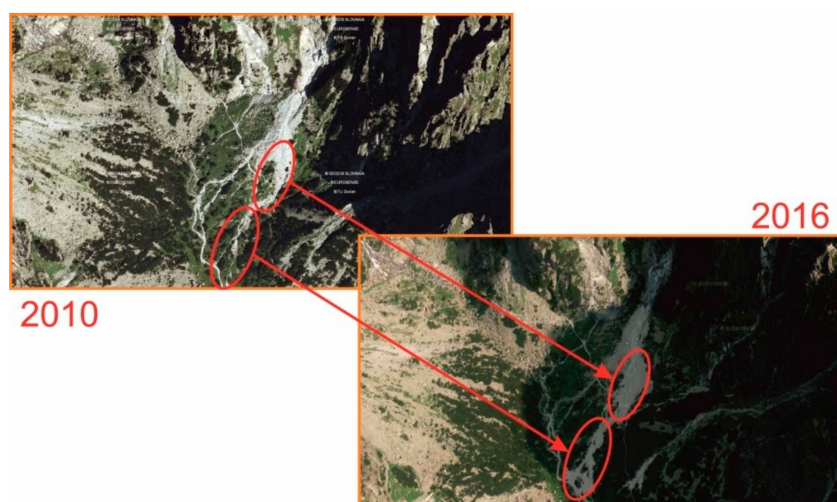


Figure 2. Visible changes in the monitored talus cone in the Little Cold Valley, High Tatras, Slovakia. Aerial photos from 2010 and 2016.

3. Methods and Instruments

Long-term geodetic monitoring of selected geohazards, such as rock collapses, glacier moraine, stone fields, mass movement, using conventional geodetic methods and instruments (total station or 3D laser scanner) is a technically and physically very demanding process. To verify the methodology and the possibility of monitoring geohazards and especially stone fields, rock collapses, and rubble cones, located in very specific, rugged, and inclined terrains in the medium-high Alpine-type mountains, the Small Cold Valley in the High Tatras, Slovakia was chosen. This valley was selected as a typical alpine landscape, with typical glacial morphology and occurrence of typical geologic phenomena, including the occurrence of Alpine-similar vegetation. At the end of the valley, there is a rubble stream (below the walls of Lomnický Peak, Figure 3).

This stream was monitored in this research by methods of mass data collection—tested method low-cost UAS photogrammetry. Trusted reference measurements were performed by 3D terrestrial laser scanning. We used the approach for the UAS data collection and process workflow for the needs of georelief modelling described in [34] (Figure 4), carried out in five basic steps:

1. Terrain reconnaissance;
2. Preparatory work and pre-flight preparation;
3. Photogrammetric data collection;
4. Processing of aerial images;
5. Creation of terrain model.

During processing, Agisoft Photoscan uses camera calibration parameters (elements of interior orientation) based besides ground control points also on key points. Hence, the calibration is based on a high number of points for each individual image (thousands: in the settings, 40,000 points per image were set as a maximum). In Figure 4, Step 2, pre-flight calibration of the camera is shown as an option. In our study, we used a post-processing camera calibration feature in Agisoft Photoscan.



Figure 3. A documented active talus cone in the Little Cold Valley, High Tatras, Slovakia.

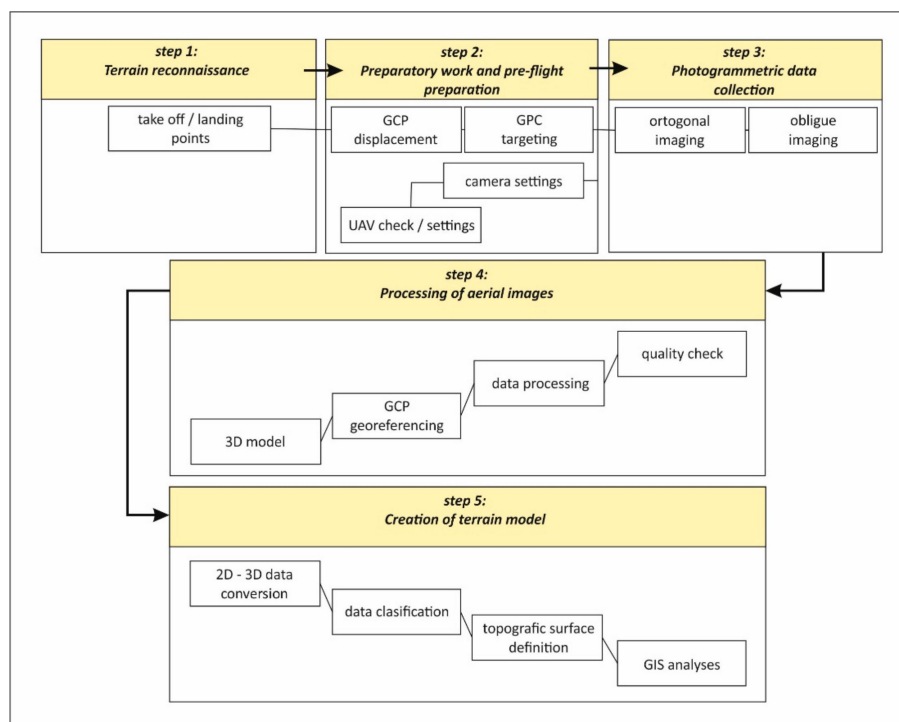


Figure 4. Example of data collection methodology using unmanned aerial system (UAS) for modeling georelief, according to [33].

It was necessary to build a precise geodetic network for research purposes. The geodetic network was stabilized by four copper studs (affixed into the rock using Fischer chemical mortar) and three reflective targets (reflective foils) glued with a special adhesive (Pattex Chemoprén Universal) to suitable flat rock surfaces or large stone blocks (see Figure 5 for locations). There were also three temporary points measured using GNSS RTK (Real Time Kinematic) method with connection to the Leica SmartNet network, which formally served to connect a geodetic network to local Datum of Uniform Trigonometric Cadastral Network and height above sea level (Baltic Vertical Datum—After Adjustment). GNSS measurements were made by a Leica GPS900cs receiver. Temporary GNSS points

were used only to determine the spatial position of the total station, and then everything was measured by the spatial polar method (geodetic network, UAS ground control points, scanner ground control points). Geodetic measurements were performed by a total station of Leica TS02 (Figure 6, left; Table 1) with an angular accuracy of $7''$ (0.0020 gon) and a length accuracy of $2 + 2$ ppm. The measurement was performed using two telescope faces from a single station. The spatial accuracy (standard deviation) of the individual points was below 10 mm. During measurements, the spatial position of the total station was checked regularly.



Figure 5. Geodetic network (crosses mark the points of geodetic network and the arrow indicates the position of the total station. Source of map: maps.google.com).



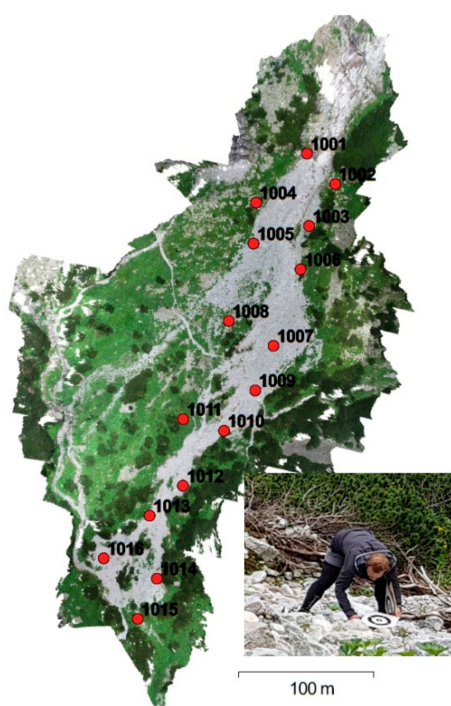
Figure 6. Leica TS02 total station (left), DJI Phantom 4 Pro (middle), and 3D scanner Leica P40 (right).

The UAS DJI Phantom 4 Pro (Figure 6, middle) equipped with a 5472×3648 pixel camera was used to capture the images of the talus cone. Altogether, 1389 images were taken in several flights from an average height of 35 m above ground, with 1 pixel therefore representing approximately 0.01 m. The automatic camera mode with fixed ISO (100) was used during the flight (ISO 100, Shutter $1/60$ to $1/800$, $F/3.5 - F/7.1$). The total flight time was about 3 h.

Table 1. Leica TS02 characteristics.

Angle Measurements (Hz, V)	
Accuracy	7"
Compensation	Angular compensation
Length measurement with a prism	
Reach	3.500 m
Accuracy	Accurate+: 1.5 mm + 2.0 ppm, Accurate Fast: 3.0 mm + 2.0 ppm, Tracking: 3.0 mm + 2.0 ppm
Distance measurement without a prism	
Range	>400 m
Accuracy	2 mm + 2 ppm
Operation	
Operating temperature	−20 to 50 °C (−4 to 122 °F) Arctic version −35 to 50 °C (−31 to 122 °F)

The ground control points were made of fibreboard 0.3×0.3 m with a black and white target. The GCPs were prevented from dislocation by being weighted down using stones collected on site, the positions are shown in Figure 7. The image acquisition was performed in four flights due to battery endurance. The first flight was manually piloted, with the aim of maintaining a stable height above the terrain. Due to the difficulties with spatial orientation on the study site, it was guided with the help of a co-worker in a way that allowed proper coverage of the study area. The three remaining flights used an autopilot and pre-programmed flight paths (pre-programming was performed in the Pix4D software). The aim was to achieve the best possible geometry of camera positions for subsequent 3D modelling. The flight height was set to 30 m above the take-off point as the Pix4D software does not support different heights in different waypoints. To obtain images covering the entire study area from a similar distance above terrain, the study area was divided into three parts, each covering an area with a similar altitude. All flight missions used a double grid pattern; however, the last flight had to be interrupted due to a sudden worsening of meteorological conditions (strong gusts of wind): therefore, the bottom part of the area was not covered using a double grid pattern (see Figure 10, left).

**Figure 7.** Location of ground control points (red dots) and installation of a ground control point.

Terrestrial laser scanning was performed with the Leica P40 (Figure 6, right; Table 2), which has a two-axis compensator, 1.2 mm + 10 ppm accuracy of measured distance, 8" angular accuracy (0.0025 gon), 3 mm/50 m and 6 mm/100 m for 3D point accuracy, a scan speed of up to 1 million points per second and $360 \times 270^\circ$ field of view. For each scanner standpoint, at least three temporary control points (black and white targets that can be scanned automatically after selection) were measured by the total station to register the resulting point clouds. The scanner resolution was set to 12 mm/10 m with a range of 120 m.

Table 2. Leica P40 3D scanner characteristics.

Main Specification	
3D scanner characteristics	compact, pulse, dual-axis compensator
Accuracy	
Range	1.2 mm + 10 ppm
Angular	8" horizontal; 8" vertical
3D position	3 mm at 50 m; 6 mm at 100
Target acquisition	2 mm standard deviation at 50 m
Distance Measurement System	
Type	Ultra-high speed time-of-flight enhanced by Waveform Digitising (WFD) technology
Range and reflectivity	Minimum 0.4 m, 270 m@34%; 120 m@8%
Scan rate	Up to 1,000,000 points per sec
Field of view	H – 360° (max.); V – 290° (max.)
Range noise	0.4 mm rms at 10 m, 0.5 mm rms at 50 m

A total of 25 standpoints (see Figure 8) were used, with a scanning time of about 12 h, which amounted (including transport and movement in the difficult terrain) to two working days—it was difficult indeed to carry a scanner weighing around 28 kg (including batteries and a protective box) around and through the stone fields.

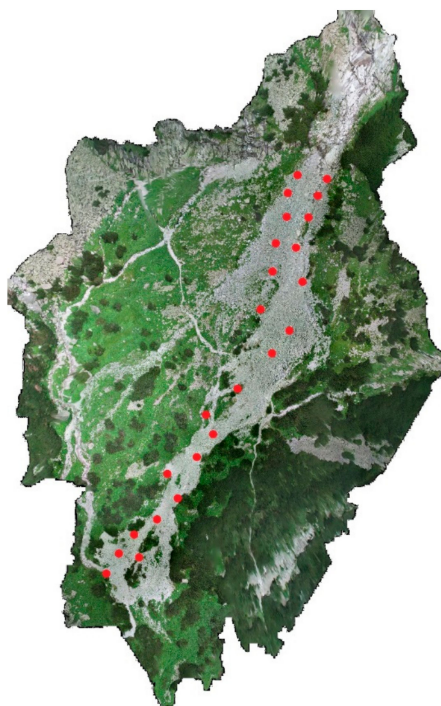


Figure 8. Leica P40 standpoints.

4. Processing of Measured Data

3D data from the laser scanner was only processed by transforming individual positions into a common coordinate system by ground control points, which were determined by the total station measurement with connection to stabilized points of the geodetic network. There was no need for further processing. The resulting point cloud contained 597 million points. The scan registration accuracy was below 3 mm in all stations. The mean RMSE (root-mean-square error) was approx. 1.2 mm.

The processing was carried out in the Leica Cyclone program. The resulting data is shown in Figure 9; Figure 9A shows measurements from one standpoint of the instrument, where, due to the character of the terrain (boulders, etc.), there are fundamental obstacles and the data itself is very incomplete. Figure 9B shows the situation after merging all the data for a given area, where the situation is already considerably better, but the terrain coverage is definitely not compact.

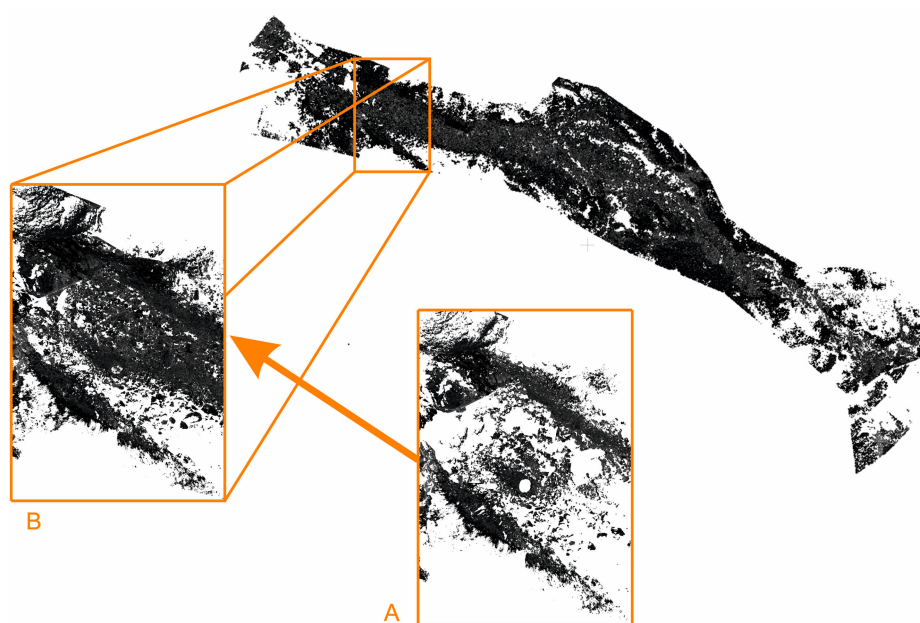


Figure 9. 3D scanning data after registration—whole area of interest. (A) Detail of data acquired from one standpoint, and (B) detail of complete data.

UAS images were processed in Agisoft PhotoScan ver. 1.2.5. A total of 1389 images were used (Figure 10, left). The processing was very problematic due to the detail level required. The calculation quality was set to “High quality” (where the original image resolution is used) when aligning images even when generating point clouds. A total of seven computers and a server in a common network solution were used for the calculation. The alignment was performed in a bulk for all frames, after which, due to computational demands, the area had to be divided into nine parts for separate generation of point clouds and the data was subsequently merged. The areas were chosen gradually so that they always remain unchanged at the two territorial boundaries. A total of 261 million points were obtained after the data was merged (Table 3).

Table 3. Numbers of points in the acquired point clouds.

Point Cloud by Method	Number of Points
SfM	261,097,729
TLS—original	597,031,328
TLS—filtered	532,956,824

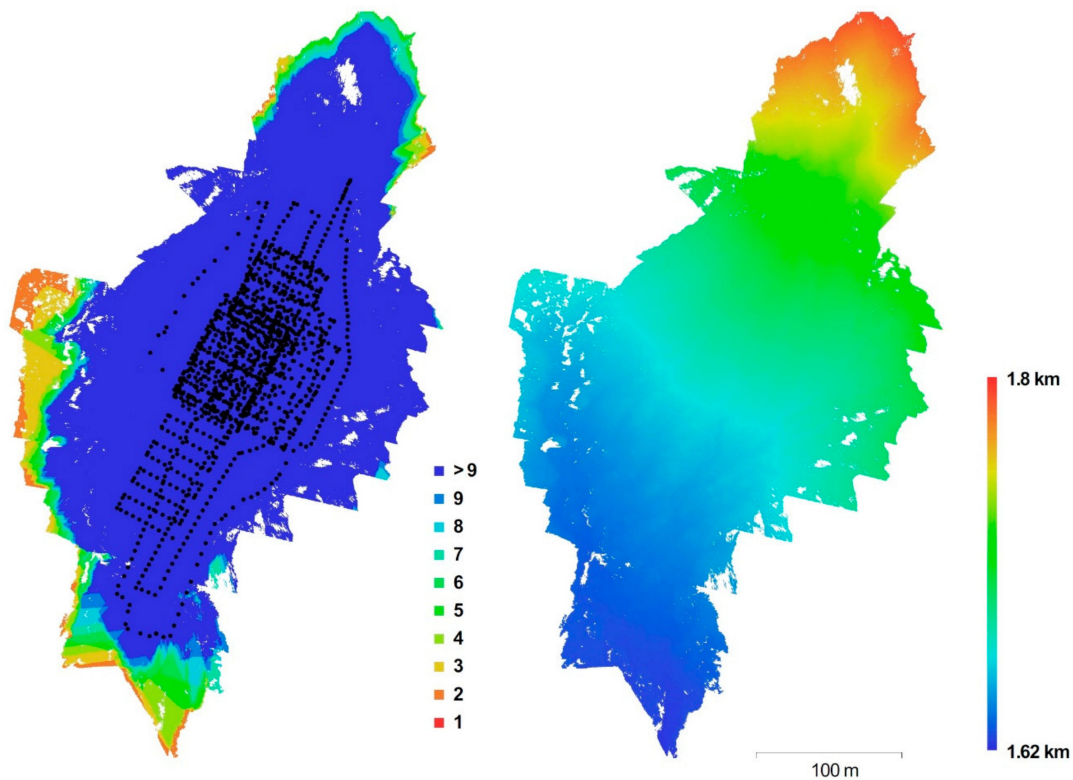


Figure 10. The number of UAS images capturing the area and the flight plan; dots represent camera positions during image acquisition (left) and reconstructed digital elevation model with the color scale shows altitudes (right).

The quality of the photogrammetric model was inspected after the calculation (Table 4). The RMSE on ground control points was less than 0.025 m and the mean overall RMSE was 0.011 m; the RMSE of image coordinates was always less than 0.32 pix and the mean RMSE of coordinates was 0.16 pix. The RMSE values characterize the internal model agreement, not the absolute accuracy of the generated point cloud. The evaluation of the SfM-derived point cloud is performed further on in the paper by a comparison with TLS results. The altitudes of the terrain are shown in Figure 10 (right). The resulting point cloud obtained from the SfM method is shown in Figure 11 depicting an overview and detail of the terrain capture. The detail of terrain capture and virtually non-creeping coverage of the area suggests greater suitability of the SfM method for such specific terrain.

Data comparison was performed in CloudCompare [35]. Due to the discontinuity of 3D laser scanning data, it was necessary to calculate the data using SfM as the reference, and to subsequently project the 3D scan data on it. If done the other way around, photogrammetrically obtained data would show high deviations in the places where 3D scan data is missing simply due to the absence of data. The points representing vegetation (shrubs, grass, and other lower small vegetation) were manually removed from the clouds before the comparison as much as possible, however some small areas of vegetation could not be manually removed.

The point clouds were directly compared by determining the minimum distance of each individual point from the TLS cloud to an irregular triangular network formed between the nearest nine points of the SfM cloud (function Cloud to Cloud, tab Local modelling, Local model option 2D1/2 Triangulation). Only comparison on the vertical axis (the only relevant one for time series analyses) was performed.

The absolute distances, as well as the individual components of this distance in the direction of the X, Y, and in particular Z coordinate axes, were calculated. The height component is very important for the resulting assessment of data quality or their mutual consent. The function “Compute cloud-to-cloud distance” was used, the components of length in the X, Y, Z directions were calculated, and the local

surface modeling using a triangular mesh made of the nearest nine points was used. The average distance (systematic shift) and the standard deviation of the differences were also calculated. To get rid of outliers that were to a large degree (besides being inherently present in any measurement) caused by islets of vegetation that could not have been manually removed and by deep shadow areas between stones, we subsequently filtered them out by removing all data where the difference between clouds was higher than $2.5 \cdot \sigma_Z$ (i.e., removing approx. 1% of the most outlying values), thus creating a filtered TLS cloud (Table 3), and repeated the accuracy evaluation of the filtered cloud as well.

Table 4. The residuals calculated for the ground control points after the bundle block adjustment.

Control Point Number	RMSE (m)	X _{error} (m)	Y _{error} (m)	Z _{error} (m)	Image (pix)
1001	0.022	−0.006	−0.021	−0.002	0.122
1002	0.013	−0.008	0.009	−0.006	0.093
1003	0.011	0.010	−0.005	0.000	0.201
1004	0.010	0.001	0.008	0.006	0.205
1005	0.021	−0.008	0.018	−0.005	0.150
1006	0.011	0.009	−0.005	0.002	0.145
1007	0.005	0.004	−0.002	0.002	0.169
1008	0.006	−0.002	0.005	0.003	0.138
1009	0.002	0.002	−0.002	0.001	0.138
1010	0.006	−0.002	−0.005	0.003	0.128
1011	0.003	0.001	−0.003	−0.002	0.168
1012	0.002	−0.001	−0.002	−0.001	0.150
1013	0.006	−0.006	−0.001	0.002	0.168
1014	0.012	0.005	−0.010	−0.006	0.183
1015	0.003	0.002	−0.002	−0.002	0.227
1016	0.016	0.000	0.016	0.004	0.318
RMSE	0.011	0.005	0.009	0.004	0.159

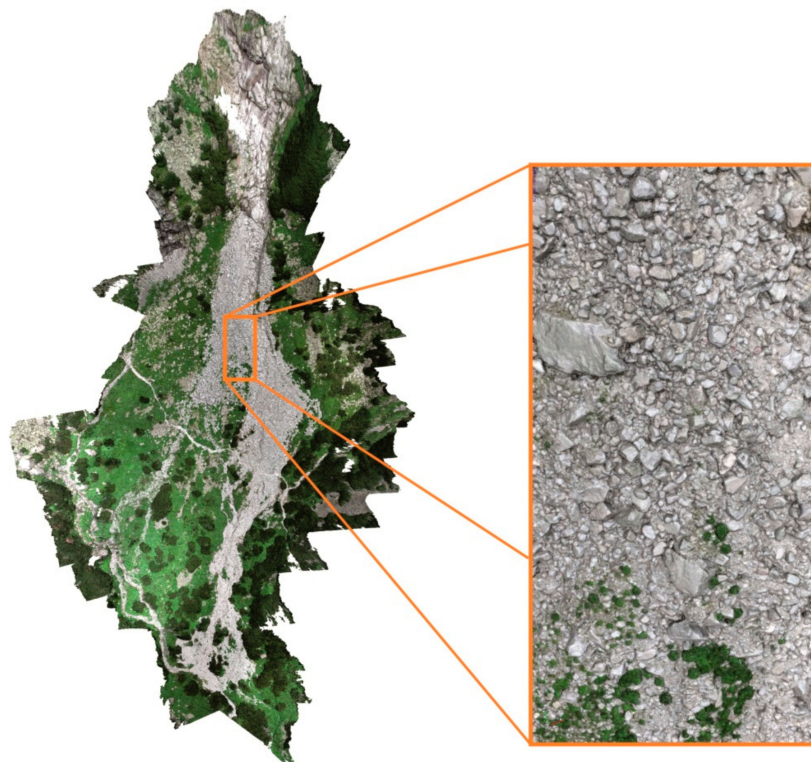


Figure 11. Data from photogrammetric image processing by SfM method—entire area and detail.

5. Results

By field research on a pre-selected site in the Little Cold Valley in the High Tatras, data capturing the same object of interest—the talus cone—were collected using two methods at the same time. Measurements were taken simultaneously—photogrammetrically from images taken via UAS from an approximate flight height of 35 m above terrain, and by terrestrial 3D laser scanning by a device placed on a tripod at approximately 1.5 m above ground. The control points were determined in both cases from the same geodetic network.

5.1. Evaluation of Precision of the Created Point Clouds

The precision of each point of the TLS point cloud related to the standpoint acquired by the 3D scanner is in our case given by the standard deviation in position less than 3 mm (according to the manufacturer's specifications, the measurement distance was shorter than 50 m). The precision of the registration was in our case characterized by the RMSE 1.2 mm. The ground control points precision was 10 mm. Total standard deviation in position of the individual point of the TLS point cloud can then be derived (by the application of the standard deviation propagation law) as 10 mm. Uncertainty added to the results by the TLS measurement itself is therefore negligible in view of the purpose of the monitoring. In contrast, the uncertainty of the SfM method point cloud generation is much higher—the point cloud is, in comparison to the TLS cloud, very noisy, as is generally known. Thus, the 3D scanning method can be considered more accurate and is used as the reference one.

The visualization of the result of the comparison of the point clouds (TLS and UAS) is shown in Figure 12, with various colors representing the differences.

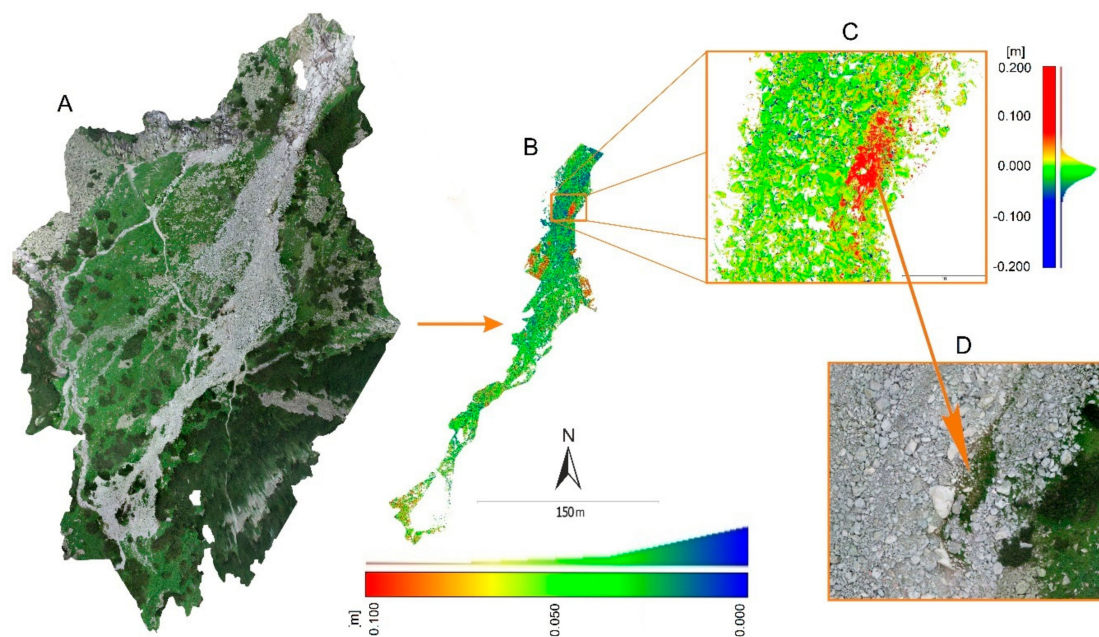


Figure 12. The result of comparing data from terrestrial 3D laser scanning and UAS photogrammetry. (A) The whole area of interest (only the talus cone of which was analyzed, the rest containing vegetation was manually removed); (B) comparison of the unfiltered clouds showing absolute differences between clouds. (C) Detail of the map of positive and negative differences and (D) its real color 3D realistic view, from which it is apparent that the differences correspond with remainders of vegetation.

The resulting cloud contains 597 million points, the average absolute distance of the clouds is 0.04 m, and the standard deviation is 0.087 m. A 0.001 m shift was determined for the Z-axis component and the standard deviation was 0.084 m. Figure 12 shows the whole captured area (Figure 12A), its analyzed part (talus cone, Figure 12B), a detail from a location where significant height deviations

have been identified on the surface of the monitored area (Figure 12C), and the 3D representation of the same part of the terrain in real colors. It is obvious that the higher deviations correspond with the areas of low vegetation (strong red color on the differences point cloud corresponds with the area of dark green dwarf pines on the 3D realistic view), while dark blue spots in Figure 12C show deviations in areas between stones where the compared methods work differently. As SfM reconstructs the area using facets and has trouble reconstructing areas of deep shadow between stones while 3D scanning directly measures distances, under such specific terrain conditions, differences between the two models may arise not due to inaccuracy, but due to the difference in the calculation (measurement) principle.

After filtering these points out from the cloud based on the size of the deviation, i.e., 0.20 m, 537 million points remained in the cloud. The reduced point cloud showed a mean absolute deviation of 0.028 m and a standard deviation at an absolute distance of 0.029 m. A mean difference of -0.008 m is practically negligible in the altitude component, and the standard deviation is 0.032 m (see Table 5).

Table 5. Comparison of the point clouds—differences in the z axis.

Differences between Methods	Mean Difference (m)	Standard Deviation (m)	Mean Absolute Difference (m)	Maximum Negative Difference (m)	Maximum Positive Difference (m)
TLS vs. SfM	0.001	0.084	0.046	-3.620	4.993
TLS vs. SfM—filtered	-0.008	0.032	0.022	-0.200^*	0.200*

Another representation of the errors present in the unfiltered cloud is shown in Figure 13. It clearly shows a cluster of outliers showing SfM overestimating the terrain by approx. 0.4 m, which exactly corresponds with the height of vegetation. Therefore, we can conclude that with the exception of vegetation-covered areas, the terrain model obtained from low-cost UAS photogrammetry achieves qualitative (precision) parameters comparable to those obtained by terrestrial laser scanning and is thus suitable as a basis for systematic monitoring that will form a basis for identification of surface changes at the centimeter level.

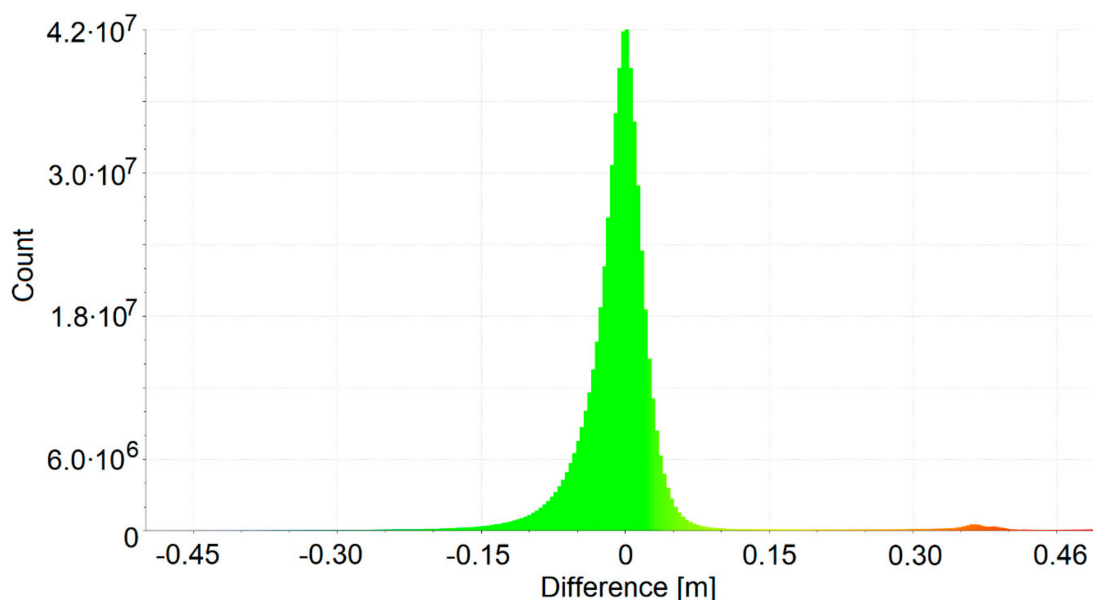


Figure 13. A histogram characterizing the distribution of the data differences in the unfiltered cloud showing a red group of outliers caused by low vegetation.

It must be also pointed out that our method directly compares point clouds rather than creating digital terrain models, creation of which requires a substantial aggregation of points and thus introduces

errors. The method used, comparing each point from one point cloud against an area formed from an irregular triangular network based on nine nearest points from the other cloud, provides in our opinion the best possible accuracy estimation.

For monitoring purposes, our method comparing SfM models from different time points will therefore provide a clear record of vertical changes in the talus cones. A geodetic network with a sub-centimeter accuracy has been established on the site, which will allow easy re-setting of ground control points and repeated monitorings will therefore be much easier and less time-consuming.

The presented results also show the importance of removing outliers when comparing data acquired using different methods. The vegetation on the one hand and deep shadow areas combined with obstacles in the way of TLS beam on the other hand resulted in differences that were in some instances very high. After removing these outliers, however, the accuracy parameters detailed in Table 5 (and thus the agreement between methods) improved considerably (where values 0.200 marked by * are given by the filter limit values). Nevertheless, for the purposes of monitoring, even unfiltered clouds would provide valuable information as it is reasonable to assume that either the location of the vegetation would remain unchanged (hence there would be no or only minuscule difference when using the same method to capture it) or, if the entire talus cone moves, the vegetation would be either buried under the rubble or moved to a new location where it would be recorded as a change from the last monitoring record. In all instances, valuable information about the mass movement would be recorded and differences that were observed in our study between two methods based on different principles (SfM and TLS) would not play a major role for real monitoring.

5.2. Efficiency and Technical Demands of Selected Geodetic Methods

In the past 10 years, terrestrial laser scanning has found a solid place in various areas of geodesy, where the object of interest—the surface of objects or terrain—is documented in detail. When using TLS, the process of data retrieval consists of:

- Terrain reconnaissance and point field creation;
- Preparation of the instrument on the standpoint and subsequent scanning process;
- Processing of the measurements.

The time period for individual steps lasts for tens of minutes to hours, while the most demanding part is processing field measurements into the final model. In our case, due to the character of the terrain, the whole field data collection representing the transport of the scanner to the site and its movement on the rubble cone was very demanding both technically and physically. The terrestrial laser scanner is one of the most expensive surveying devices. Its weight is approx. 28 kg including the container, and the price is about €70,000. While carrying the device between the standpoints, any slip or fall of the person carrying it or the surveyor can mean damage or destruction of the instrument. Due to complicated transportation, mountain carrying, and manipulation with the scanner in difficult terrain, performing repeated measurements is difficult at best. This, along with the terrain ruggedness, resulting in obstruction of the terrain by terrain features closer to the scanner, speaks against the use of this technology in mountain conditions.

In this field, the opposite of using TLS is the use of cheap UAS carriers. Transport of this technology over the mountain terrain is incomparably easier. The cost of a “cheap” UAS is around €1500 and the weight is about 3 kg, which is a fraction of the price and weight of the TLS. Overall, from the point of view of efficiency and technical difficulty, repeated monitoring by using low-cost UAS photogrammetry is a much preferable method for collecting data in mountain conditions.

5.3. Suitability of Used Geodetic Methods to Monitor Dynamics of the Development of the Georelief

For real use of selected geodetic methods and instruments, based on the achieved results, it should be pointed out that despite the expected decreased accuracy of low-cost UAS photogrammetry, UAS imaging and subsequent SfM image processing are a significantly better choice than TLS. In addition

to being an easier and less time-consuming measurement, it also offers a complex coverage of the monitored area without “holes” in the point cloud, and includes very good color information to allow easy interpretation of the detected shifts. In terms of laboriousness, there is a big difference between methods—drone imaging, including stabilization of control points, took about 3 h. Apart from the stabilization of control points mentioned above, it is not necessary to move in the monitored area, which is extremely advantageous due to its surface. In contrast, 3D terrestrial scanning took two working days, and the movement in the stone field with the measuring technique was physically very demanding and lengthy, which makes UAS a significantly more economical solution. Speaking of the economical side of model acquisition, the equipment for low-cost drone imaging is also significantly cheaper. While the hardware and software costs were below €5000 in the configuration used, it amounts to approx. €100,000 in the case of 3D scanning (both without geodetic instruments for geodetic surveying, network and control points).

Besides, when using TLS scanning, the terrain morphology and the need to scan even from low attitudes causes discontinuous terrain capture due to many obstructions from nearby large boulders when creating the final point cloud.

Another advantage of the UAS photogrammetry is the production of high-resolution ortho-photos in addition to point clouds, which facilitates visual identification of changes.

In our study, we did not attempt to record any temporal changes in the mass movement but aimed at developing methods for future recording of such changes. Although the accuracy of both tested methods is sufficient for intended monitoring of changes, it must be taken into account that due to differences in measurement and data processing, the model can produce apparent changes that are not substantiated. Each of these technologies is, on its own, sufficiently accurate given the accuracy, but according to efficiency and overall suitability of the methods for demanding high-altitude conditions and the appearance of the other parameters described above, it is unambiguously recommended to use the more suitable drone imaging method, which is fast, sufficiently accurate, and environmentally friendly. It would be interesting to try 3D scanning from the drone for this purpose, but this would be associated with significantly higher input costs and again introduce a risk of damaging very expensive equipment. Besides, airborne 3D scanners are substantially heavier than a simple camera and would require a drone with a higher load capacity, which would be associated with higher noise generation. Operating such a noisy drone would be, especially in the tranquil environment of the national park, highly undesirable.

6. Conclusions

In our study, we have shown that in difficult mountain conditions, UAS photogrammetry is capable of providing models of comparable quality with those acquired by TLS for monitoring movement of the talus cones. Taking into account the ease of data acquisition, equipment costs, and risk of damage of the expensive TLS equipment, UAS photogrammetry appears to be an ideal method for repeated monitoring of geological phenomena in a very rugged mountainous terrain due to its accuracy, low cost, ease of application, and efficiency, plus it is technically unassuming.

Our method used a direct comparison of point clouds rather than creating digital terrain models that inherently require some level of approximation, thus introducing error. Besides, although we demonstrated the level of improvement of the agreement between TLS and SfM by filtering out outliers (mostly caused by remnants of vegetation in the talus cone or by principal differences between the way both methods operate), real monitoring would only use the SfM method and as such, recording the changes (i.e., mass movement) would in all likelihood work very well even without this filtering out of outliers as both above reasons for the error would be prevented.

Author Contributions: Conceptualization, R.U. and M.Š.; Methodology, P.B., L.K., S.J., I.Đ.; Software, M.Š.; Validation, R.U., P.B. and L.K.; Formal Analysis, M.K. and S.S.; Investigation, R.U., M.Š., P.B., L.K. and S.J.; Resources, M.Š. and P.B.; Data Curation, P.B., M.P. and I.Đ.; Writing—Original Draft Preparation, R.U. and M.Š.;

Writing—Review and Editing, R.U. and M.Š.; Visualization, P.B.; Supervision, P.B.; Project Administration, P.B.; Funding Acquisition, M.K. and S.S.

Funding: This research was funded by: Grant Agency of CTU in Prague—grant number SGS19/047/OHK1/1T/11, Scientific Grant Agency of the Slovak Republic (VEGA – MŠVVaŠ SR—grant number 1/0844/18 and supported by project SKHU/1601/4.1/187.

Acknowledgments: This study would not have been possible without the support of the National Park—TANAP.

Conflicts of Interest: The authors declare no conflict of interest. The funders had no role in the design of the study; in the collection, analyses, or interpretation of data; in the writing of the manuscript, or in the decision to publish the results.

References

- Braun, J.; Hánek, P. Geodetic Monitoring Methods of Landslide-Prone Regions—Application to Rabenov. *Acta Universitatis Carolinae Geographica* **2014**, *49*, 5–19. [\[CrossRef\]](#)
- Barbarella, M.; Fiani, M. Monitoring of large landslides by terrestrial laserscanning techniques: Field data collection and processing. *Eur. J. Remote Sens.* **2013**, *46*, 126–151. [\[CrossRef\]](#)
- Bitelli, G.; Dubbini, M.; Zanutta, A. Terrestrial Laserscanning and Digital Photogrammetry Techniques to Monitor Landslide Bodies. In Proceedings of the XX-th ISPRS Congress: Commission V, Istanbul, Turkey, 12–24 July 2004; pp. 246–251.
- Derrien, A.; Villeneuve, N.; Peltier, A.; Beauducel, F. Retrieving 65 years of volcano summit deformation from multitemporal structure from motion: The case of Piton de la Fournaise (La Réunion Island). *Geophys. Res. Lett.* **2015**, *42*, 6959–6966. [\[CrossRef\]](#)
- Jovančević, S.D.; Peranić, J.; Ružić, I.; Arbanas, Ž. Analysis of a historical landslide in the Rječina River Valley, Croatia. *Geoenviro. Disasters* **2016**. [\[CrossRef\]](#)
- Rossi, G.; Tanteri, L.; Tofani, V.; Vannocci, P. Multitemporal UAV surveys for landslide mapping and characterization. *Landslides* **2018**, *15*, 1045. [\[CrossRef\]](#)
- Ridolfi, E.; Buffi, G.; Venturi, S.; Manciola, P. accuracy analysis of a dam model from drone surveys. *Sensors* **2017**, *17*, 1777. [\[CrossRef\]](#)
- Buffi, G.; Manciola, P.; Grassi, S.; Barberini, M.; Gambi, A. Survey of the Ridracoli Dam: UAV-based photogrammetry and traditional topographic techniques in the inspection of vertical structures. *Geomat. Nat. Hazards Risk* **2017**, 1562–1579. [\[CrossRef\]](#)
- Duró, G.; Crosato, A.; Kleinhans, M.G.; Uijttewaal, W.S.J. Bank erosion processes measured with UAV-SfM along complex banklines of a straight mid-sized river reach. *Earth Surf. Dyn.* **2018**, *6*, 933–953. [\[CrossRef\]](#)
- Peppas, M.V.; Mills, J.P.; Moore, P.; Miller, P.E.; Chambers, J.E. Brief communication: Landslide motion from cross correlation of UAV-derived morphological attributes. *Nat. Hazards Earth Syst. Sci.* **2017**, *17*, 2143–2150. [\[CrossRef\]](#)
- Salvini, R.; Mastrorocco, G.; Esposito, G.; Di Bartolo, S.; Coggan, J.; Vanneschi, C. Use of a remotely piloted aircraft system for hazard assessment in a rocky mining area (Lucca, Italy). *Nat. Hazards Earth Syst. Sci.* **2018**, *18*, 287–302. [\[CrossRef\]](#)
- Kovacevic, M.S.; Car, M.; Bacic, M.; Stipanovic, I.; Gavin, K.; Noren-Cosgriff, K.; Kaynia, A. *Report on the Use of Remote Monitoring for Slope Stability Assessments; H2020-MG 2014-2015; Innovations and Networks Executive Agency: Zagreb, Croatia, 2015.*
- Kaufmann, V.; Seier, G.; Sulzer, W.; Wecht, M.; Liu, Q.; Lauk, G.; Maurer, M. Rock Glacier Monitoring Using Aerial Photographs: Conventional vs. UAV-Based Mapping—A Comparative Study. *Int. Arch. Photogram. Remote Sens. Spatial Inf. Sci.* **2018**, *XLII-1*, 239–246. [\[CrossRef\]](#)
- Vivero, S.; Lambiel, C.H. Monitoring the crisis of a rock glacier with repeated UAV surveys. *Geogr. Helv.* **2019**, *74*, 59–69. [\[CrossRef\]](#)
- Kohút, M.; Janák, M. Granitoids of the Tatra Mts., Western Carpathians: field relations and petrogenetic implications. *Geol. Carpath.* **1994**, *45*, 301–311.
- Petrík, I.; Nabelek, P.L.; Janák, M.; Plašienka, D. Conditions of Formation and Crystallization Kinetics of Highly Oxidized Pseudotachylytes from the High Tatras (Slovakia). *J. Petrol.* **2003**, *44*, 901–927. [\[CrossRef\]](#)

17. Lukniš, M. The course of the last glaciation of the Western Carpathians in the relation to the Alps, to the glaciation of northern Europe, and todivision of central European Würm into periods. *Geografický Casopis* **1964**, *16*, 127–142.
18. Klimaszewski, M. *Relief of the Polish Tatra Mountains*; Panstwowe Wydawnictwo Naukowe: Warszawa, Poland, 1988.
19. Lindner, L.; Dzierzek, J.; Marciniak, B.; Nitychoruk, J. Outline of Quaternary glaciations in the Tatra Mts.: their development age and limits. *Geol. Q.* **2003**, *47*, 269–280.
20. Zasadni, J.; Klapysa, P. The Tatra Mountains during the Last Glacial Maximum. *J. Maps* **2014**, *10*, 440–456. [[CrossRef](#)]
21. Kotarba, A.; Strömquist, L. Transport, sorting and deposition processes in the Polish Tatra Mountains. *Geogr. Ann.* **1984**, *66*, 285–294. [[CrossRef](#)]
22. Kotarba, A.; Kaszowski, L.; Krzemień, K. *High-Mountain Denudational System in the Polish Tatra Mountains*; Ossolineum: Wroclaw, Poland, 1987; pp. 1–106.
23. Sass, O.; Krautblatter, M. Debris-flow-dominated and rockfall-dominated scree slopes: genetic models derived from GPR measurements. *Geomorphology* **2007**, *86*, 176–192. [[CrossRef](#)]
24. Fort, M.; Cossart, E.; Deline, P.; Dzikowski, M.; Nicoud, G.; Ravel, L.; Schoeneich, P.; Wassmer, P. Geomorphic impacts of large and rapid mass movements: a review. *Geomorphologie* **2009**, *1*, 47–63. [[CrossRef](#)]
25. Krautblatter, M.; Moser, M.; Schrott, L.; Wolf, J.; Morche, D. Significance of rockfall magnitude and carbonate dissolution for rock slope erosion and geomorphic work on Alpine limestone cliffs (Reintal, German Alps). *Geomorphology* **2012**, *167–168*, 21–34. [[CrossRef](#)]
26. Lukniš, M. *Reliéf Vysokých Tatier a Ich Predpolia*; Vydavateľstvo SAV: Bratislava, Slovak, 1973; p. 375.
27. Zimmerman, M.; Haeberl, I.W. Climate change and debris flow activity in the highmountain areas—A case study in the Swiss Alps. *Catena Suppl.* **1990**, *22*, 59–72.
28. Kotarba, A. Formation of high mountain talus slope related to debris-flow activity in the High Tatra Mountains. *Permafrost Periglacial Processes* **1997**, *8*, 191–204. [[CrossRef](#)]
29. Anderson, R.S. Modeling the tor-dotted crests, bedrock edges, and parabolic profiles of high alpine surfaces of the Wind River Range, Wyoming. *Geomorphology* **2002**, *46*, 35–58. [[CrossRef](#)]
30. Melo, M.; Lapin, M.; Pecho, J.; Kružicová, H. Climate Trends in the Slovak Part of the Carpathians. In *The Carpathians: Integrating Nature and Society Towards Sustainability*; Springer: Berlin/Heidelberg, Germany, 2013; ISBN 978-3-642-12724-3. [[CrossRef](#)]
31. Kotarba, A. Geomorphic Processes and Vegetation Pattern Changes. Case Study in the Zelené Pleso Valley, High Tatra, Slovakia. *Studia Geomorphol. Carpatho Balcanica* **2005**, *39*, 39–48.
32. Van Steijn, H. Debris-flow magnitude-frequency relationships for mountainous regions of central and northwest Europe. *Geomorphology* **1996**, *15*, 259–273. [[CrossRef](#)]
33. Niedźwiedz, T. Extreme Precipitation Events on the Northern Side of the Tatra Mountains. *Geogr. Polonica* **2003**, *76*, 15–23.
34. Rusnák, M.; Sládek, J.; Kidova, A.; Lehotský, M. Template for high-resolution river landscape mapping using UAV technology. *Measurement* **2018**, *115*. [[CrossRef](#)]
35. Software CloudCompare. Available online: www.cloudcompare.org (accessed on 10 April 2019).

